

## Modeling of a carbon nanotube ultracapacitor

This article has been downloaded from IOPscience. Please scroll down to see the full text article.

2012 Nanotechnology 23 095401

(<http://iopscience.iop.org/0957-4484/23/9/095401>)

View [the table of contents for this issue](#), or go to the [journal homepage](#) for more

Download details:

IP Address: 12.203.210.10

The article was downloaded on 13/02/2012 at 19:44

Please note that [terms and conditions apply](#).

# Modeling of a carbon nanotube ultracapacitor

Antonios Orphanou<sup>1</sup>, Toshishige Yamada<sup>1,2</sup> and Cary Y Yang<sup>1</sup>

<sup>1</sup> Center for Nanostructures, Santa Clara University, Santa Clara, CA 95053, USA

<sup>2</sup> Department of Electrical Engineering, Baskin School of Engineering, University of California, Santa Cruz, 95064, USA

E-mail: [aorphanou@scu.edu](mailto:aorphanou@scu.edu) and [tyamada@scu.edu](mailto:tyamada@scu.edu)

Received 30 August 2011, in final form 5 December 2011

Published 6 February 2012

Online at [stacks.iop.org/Nano/23/095401](http://stacks.iop.org/Nano/23/095401)

## Abstract

The modeling of carbon nanotube ultracapacitor (CNU) performance based on the simulation of electrolyte ion motion between the cathode and the anode is described. Using a molecular dynamics (MD) approach, the equilibrium positions of the electrode charges interacting through the Coulomb potential are determined, which in turn yield the equipotential surface and electric field associated with the capacitor. With an applied ac voltage, the current is computed based on the nanotube and electrolyte particle distribution and interaction, resulting in the frequency-dependent impedance  $Z(\omega)$ . From the current and impedance profiles, the Nyquist and cyclic voltammetry (CV) plots are then extracted. The results of these calculations compare well with existing experimental data. A lumped-element equivalent circuit for the CNU is proposed and the impedance computed from this circuit correlates well with the simulated and measured impedances.

(Some figures may appear in colour only in the online journal)

## 1. Introduction

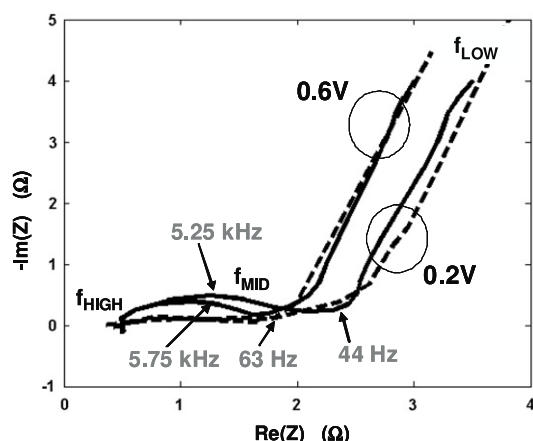
The study of ultracapacitors (UCs) or supercapacitors has been the subject of intense research in recent years [1–12]. Increase of the electrode surface area  $S$  to maximize the stored energy using capacitors has always been a prohibitive challenge. Conventional capacitors generally possess a very high power density but a low energy density, typically in the 0.01–0.05 W h kg<sup>-1</sup> range [4], making them unsuitable for high-performance energy storage applications. It has recently been reported that by using nanocarbon (graphene) to increase  $S$ , UCs can yield as much as 86 W h kg<sup>-1</sup> [5], thus demonstrating significant potential for nanocarbon UCs. In addition, vertically or randomly oriented grown carbon nanotube (CNT) arrays have been shown to increase  $S$  and the capacitor energy storage capacity drastically [13–16]. Such a technological breakthrough will have immense implications in consumer electronics and telecommunication, stand-by power systems, and electric/hybrid vehicles.

Figure 1 shows the measured Nyquist plots for a carbon nanotube ultracapacitor (CNU) at two applied voltages. Our simulation results are also shown in the same figure, and will

be discussed later. A Nyquist plot displays the capacitor's frequency-dependent reactance  $-\text{Im}(Z)$  as a function of resistance  $\text{Re}(Z)$ , with the applied voltage frequency as a parameter. The plot was obtained from electrical impedance spectroscopy (EIS) measurements for a CNU consisting of a 6 mol l<sup>-1</sup> KOH electrolyte solution subject to an applied voltage [17].

Figure 2(a) shows the experimental cyclic voltammetry (CV) plot for the same capacitor obtained using a voltage sweep rate of 1 mV s<sup>-1</sup> [17]. It displays the total current through the capacitor as a function of voltage. Figure 2(b) illustrates the simulated CV plots for a CNU with the same electrolyte ion volume density  $N_e$  as the experimental one, which will be discussed later. In CV measurements, the capacitor is linearly charged with time and subsequently allowed to discharge, providing information about the total capacitance and the capacitor's ability to store energy between the electrolyte ions and electrodes [18]. Both the CV and the Nyquist plots characterize the capacitor's electrical performance and are examined in this paper.

The analysis of ultracapacitor operation reported in the literature thus far is quite primitive and phenomenological,



**Figure 1.** Experimental and simulated Nyquist plots for a CNU with  $6 \text{ mol l}^{-1}$  of KOH electrolyte at 0.6 and at 0.2 V. Simulated and measured results are shown by dashed and solid lines, respectively. The three frequency regimes are identified by  $f_{\text{LOW}}$ ,  $f_{\text{MID}}$ , and  $f_{\text{HIGH}}$ , respectively. Two points on each experimental plot are indicated by their respective frequencies [17].

using an equivalent circuit model consisting of capacitors and resistors to simply fit the measured Nyquist plot [17]. There are no detailed science-based models explaining how the electrolyte ions move under the influence of charges on the plates, leading to the measured electrical behavior. The absence of science-based modeling makes the design of the UC cell at best empirical and heavily dependent on trial-and-error. For successful development of such a potentially far-reaching and timely technology, modeling based on sound scientific understanding must be carried out.

In addition to the complex geometry of the CNU, the electric field singularity at the tips of the nanotube makes the direct solution (analytical or numerical) of the Poisson's equation in the capacitor cell rather challenging. With molecular dynamics [19], we distribute electrode charges throughout the complex CNU structure. Then we solve for the ionic motion inside the CNU and calculate the total current, thus providing us with the degrees of freedom necessary to optimize the cell design based on CNT size and density, electrode separation/size, and applied voltage.

## 2. Simulation method

One of the challenges in developing a molecular dynamics simulation environment is the approximation of the physical 3D vertically grown CNT array with an appropriate model. In our approach, the 3D CNT 'forest' is approximated by a 2D equivalent. The justification of this dimensional transformation is the assumption that transport is channeled only in the direction normal to the electrode's perfectly reflecting walls at either end of the simulation cell, while neglecting transport in the transverse directions. For our study we assume vertically grown CNTs, but in general our methodology can assume any arbitrary CNT orientation with respect to the electrode walls. In addition, boundary condition selection is critical not only in ensuring electrical interaction exists between adjacent CNT unit cells but also

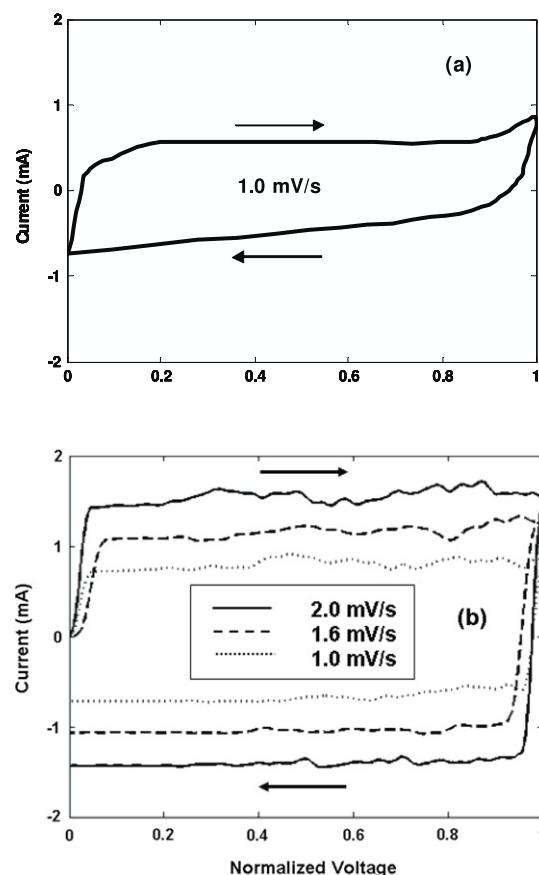


**Figure 2.** Simulated and measured CV plots. (a) Measured CV plot for an electrolyte concentration of  $6 \text{ mol l}^{-1}$  and at a voltage ramp rate of  $1.0 \text{ mV s}^{-1}$  [17]. (b) Simulated CV plots for the same electrolyte concentration and at voltage ramp rates of  $1.0 \text{ mV s}^{-1}$ ,  $1.6 \text{ mV s}^{-1}$ , and  $2.0 \text{ mV s}^{-1}$ , respectively.

conservation of energy in the CNU volume that results in a stable computational process.

Our simulation model is particle-based. The current is evaluated based on the motion of the electrolyte ions (convection current, or summation of drift and diffusion currents) and charging/discharging of the CNU plates (displacement current). There are two forces acting on an ion. One is the Coulomb force and the other is the friction force. The Coulomb force is considered based on Coulomb's law over all possible pairs of charges. The CNU plates are charged/discharged during the operation. Plate charges appear or disappear during the operation and create an electric field inside the CNU. Other ions also contribute to the field. The Coulomb force for the ion is determined by this electric field representing all the pair-wise Coulomb contributions, and is evaluated based on the molecular dynamics (MD) technique. The way in which this electric field is calculated is discussed in detail in the appendix. The other force is the friction force, and this is considered in a half-empirical way. The ion collides with water molecules or other ions and this is the origin of the friction. Even after removing the Coulomb components, there is still a friction force between ions because they have finite sizes and cannot move freely. Instead of explicitly considering the ion and water molecule

sizes, analyzing the forces between them, and examining the ion motion dynamics, we have expressed the friction in terms of the frequency-dependent collision time  $\tau(\omega)$ .  $\tau(\omega)$  is related to the mobility  $\mu(\omega) = q\tau(\omega)/m_i$  and the mobility is related to the conductance  $\sigma(\omega) = qn_i\mu(\omega)$ , where  $q$  is the unit ion charge,  $m_i$  is the ion mass, and  $n_i$  is the ion concentration. The summation of such a conductance for  $K^+$  and  $OH^-$  is the inverse of the measured resistance. Thus, the force acting on the ion is calculated by adding all the Coulomb forces, and the friction is expressed by the collision time  $\tau(\omega)$  obtained from the experimental Nyquist data  $\text{Re} Z(\omega)$ . All the details of the collision physics are embedded in the empirical quantity  $\tau(\omega)$ . Since the frequency dependence is not generally large, it is acceptable to replace  $\tau(\omega)$  with  $\tau(0)$  if no Nyquist data are available in advance.

In our simulation, the CNTs are idealized in that (1) the ions are much smaller than the CNT diameter or CNT–CNT separation, and they cannot move into the CNTs, and (2) there is no chemical reaction between the ions and the CNT surface and, therefore, once an ion sticks to the CNT surface, the force required to pull it out is the Coulomb force between the ion and plate charges. Another way to describe the situation is that there is no activation energy for an ion to leave the CNT surface. Regarding (1), the ions are of the order of 0.1–0.5 nm [20] and a typical CNT diameter ranges from  $10^{-2}$  to 1  $\mu\text{m}$  [21]. Thus, (1) is a practical assumption. Regarding (2), there are no available data for a possible reaction between the  $K^+/OH^-$  ions and the CNT surface. However, it is known that CNT surfaces are often chemically inert, as discussed in the interaction of the CNT and oxygen molecules [22, 23] or in the interaction between the CNT and ammonia molecules [24, 25]. In this sense, (2) is not a bad assumption.

The simulation is a two-step iterative process: first, the charge distribution on each CNT electrode is calculated using a full MD solution, and, second, the calculated electrode charge distribution is allowed to interact with the electrolyte ions yielding the desired CNU electrical characteristics. Details of the methodology are described in the appendix. We must scale the experimental electrolyte ion volume density  $N_e$  of KOH and CNU dimensions to our simulated unit cell. Such scaling is also described in the appendix.

### 3. Results and discussion

The experimental Nyquist plots shown in figure 1 were obtained at open-circuit peak sinusoidal voltages (OCVs) of 0.2 V and 0.6 V [17], respectively. They describe the capacitor's reactance versus resistance behavior in different frequency regimes, with the far right of the plot being the low-frequency and the left being the high-frequency impedance responses. As observed from these plots, the simulated results compare well with their experimental counterparts. Similar results were obtained in [26–30], and we use [17] as the experimental data to compare with our simulation. Using the existing phenomenological models [4], such a direct comparison would not have been possible.

In the simulation, the double layer capacitance (DLC), resulting from the electrode and the electrolyte ion charges,

is used to describe the CNU behavior. The DLC has a maximum value for dc, when the electrolyte ions are closely attached to their respective electrodes. It is responsible for the large amount of energy stored in the capacitor and is frequency-dependent, as shown in figure 1.

Our simulation results reveal that the higher the OCV is, the higher the frequency at which the DLC vanishes is. At higher OCVs, the electrolyte ions tend to maintain a close proximity to the electrodes, thus creating a larger DLC, which is less sensitive to frequency variations as shown in figure 1. As a result, a higher frequency is required to counter the added inertia of the electrolyte ions due to the presence of a higher electrode force. The straight and rigid large-diameter nanotubes used as electrodes in the experimental data [17] were obtained by chemical vapor deposition (CVD) of propylene at 800 °C within the pores of an alumina template (P800AL) and were arbitrary in orientation.

The measured CV plot [17] at a voltage ramp rate of  $1.0 \text{ mV s}^{-1}$  is shown in figure 2(a), while the simulated CV plots of the CNU cell for three different voltage ramp rates, 1.0, 1.6, and  $2.0 \text{ mV s}^{-1}$ , are shown in figure 2(b). The simulated results show that the displacement current in the CNU increases with increasing voltage. Overall, the simulated CV plot is qualitatively consistent with the measured data [16]. While the CV plots offer some insight into the CNU's charging and discharging characteristics, they do not provide any frequency dependence information. As mentioned above, the CNT in our simulation model is ideal, with the effects of the hollow channel, mesopores, defects, and surface roughness ignored. Further, we only assume that the electrical double layer is a result of the pure ionic electrostatic attractions in the capacitor (Faradaic pseudo-capacitance reactions are ignored). Thus, the CV plot is almost rectangular, indicating that the CNT electrodes are very well suited for large energy storage.

At very low frequencies, the electrolyte ions can screen the electrode charges almost perfectly, as shown in figure 3(a), and maximize the double layer energy storage in the capacitor by reducing the ion–electrode separation. In this frequency region, the electrolyte ions are well separated leading to two well-defined double layer capacitances and a maximum average free charge polarization distance,  $P(f)$ , as shown in figure 3(a). Current continuity in the CNU is thus achieved through a strong capacitive drift convection current density, which is capacitive in nature, a 'parasitic' Ohmic-drift current correction, and a very weak displacement current density. When  $\max\{P(f)\}$  is reached at low frequencies, the electric field between the CNTs is very small, resulting in a small electrolyte–electrolyte ion capacitance  $C_0$  and a weak displacement force. A limiting case of the low-frequency scenario is the CV plot of figure 2. At an extremely slowly changing voltage the ions are completely attached to their respective electrodes and unable to drift. In this scenario the current continuity in the capacitor volume is achieved through a displacement current and a very weak drift current correction.

At intermediate frequencies, the CNU still continues to exhibit capacitive characteristics. However, at this stage,

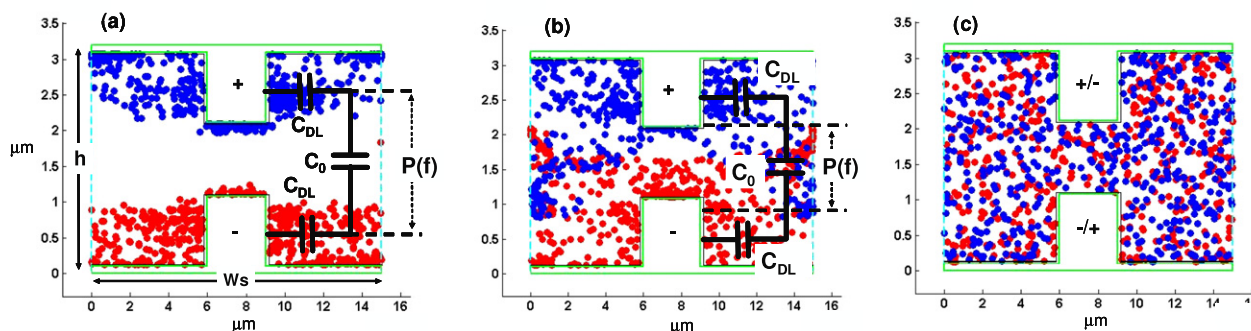


**Figure 3.** Ionic distribution snapshots at (a) low, (b) mid, and (c) high frequencies in the simulated unit cell at 0.6 V, where the CNT electrodes are situated at opposite walls of the cell indicated by green lines. Negative charges are denoted in blue and positive ones in red.  $C_{DL}$  is the double layer capacitance,  $C_0$  the capacitance between the oppositely charged electrolyte ions, and  $P(f)$  the electrolyte ion average polarization distance.

the electrolyte ions move farther away from the electrodes, as shown in figure 3(b), yielding a smaller  $C_{DL}$ . Here the electrolyte ions are at their peak drift position, farther away from the electrodes and decreasing as the capacitance decreases (the average free charge polarization distance in the capacitor volume is now smaller than in the low-frequency case). Although the capacitance due to the electrolyte ions,  $C_0$ , is now larger, the decrease in  $C_{DL}$  is much more dramatic, resulting in an overall decrease in the total capacitance. This causes the ‘bump’ in the Nyquist plots in figure 1.  $C_0$  is smallest for dc during which the electrolyte and electrode ions are closest together, maximizing the distance of the ions and minimizing the total electric field. At intermediate frequencies, the electrolyte ions still maintain a non-uniform distribution, as shown in figure 3(b), and, unlike the low-frequency case, current continuity in the CNU is achieved only through a ‘weaker’ capacitive convection current density and stronger drift current correction. At both high and intermediate frequencies, the CNU behaves like a frequency-dependent parallel  $RC$ -circuit.

At much higher frequencies the CNU displays an inductive component. The heavy electrolyte ions can no longer follow the bias changes and the electrolyte loses its dielectric ability. The total current density in the capacitor is then dominated by inductive-convection and Ohmic-drift components. Due to the uniform distribution of the electrolyte ions shown in figure 3(c), the ability of the structure to store energy is diminished, resulting in a negligible  $C_{DL}$ . At this stage the electrolyte exhibits inductive and resistive behavior and behaves much like a series  $RL$ -circuit, because the system tends to have a voltage in the opposite direction to the current (the ions are so heavy that they cannot follow the quick change in the voltage polarity at high frequency). The high-frequency CNU characteristics are of particular interest in high-speed switching applications, where high current is needed in the MHz regime. This finding further necessitates the development of a science-based model to elucidate the frequency dependence of CNU behavior.

By extracting the CNU impedance frequency response from the Nyquist plot, the impedance of the CNU is obtained as a function of frequency, as shown in figure 4 (solid

lines). At low frequencies, as expected, the CNU has negative (capacitive) reactance and a finite, exponentially decaying resistance value. As frequency increases, the reactance becomes positive and the CNU starts to exhibit slight inductive behavior and a frequency-independent resistance. This resistance value corresponds to the one at the high-frequency end of the Nyquist plot in figure 1.

From the simulation results and following the ionic distribution discussion above, we proceed to propose two equivalent lumped-circuit models for the CNU, as given in figure 4. The impedance obtained using the first model (dashed lines in figure 4(a)) captures the resistance, inductance, and convection capacitance of the CNU. The second model (figure 4(b)) offers a slightly better fit for both the resistive and reactive components of the impedance by incorporating additional circuit elements to account for the electrolyte dielectric absorption,  $R_d$  and  $C_d$ . In the low- and mid-frequency regimes, both circuit models capture the frequency-dependent capacitive and resistive behaviors of the CNU. At high frequency, the CNU impedance is dominated by its inductance and its frequency-independent resistance.

#### 4. Conclusion

Using a scaling scheme to model the 3D CNU cell, we are able to simulate the capacitor operation. Our results demonstrate the importance of a science-based approach in modeling the CNU performance. We have developed a molecular dynamic algorithm that is used to compute the current in the CNU from the electrolyte and CNT electrode charge distributions. The total current continuity in the capacitor is achieved through a dominant convection current component, which is capacitive in nature. At low and intermediate frequencies, the electrolyte ions have a distinct polarization which gives rise to a convection current. At high frequency the electrolyte ions’ polarization vanishes and the reactance becomes inductive. Further, we have shown that the current continuity in the CV plot is dominated by displacement currents. This can be viewed as the limiting case of the low-frequency behavior where ions are idle and attached to their respective electrodes.

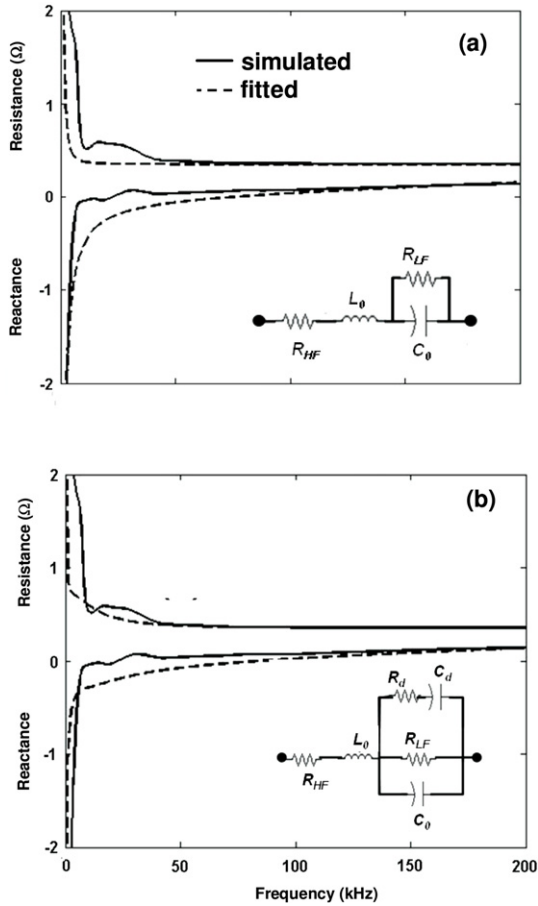


**Figure 4.** Comparison of the simulated CNU impedance with those calculated using circuit models (a) and (b). The second model yields an improved fit (dashed lines) to the simulated results (solid lines). The fitted values of the circuit elements are (a)  $L_0 = 145$  mH,  $C_0 = 35$  mF,  $R_{HF} = 0.45 \Omega$  and  $R_{LF} = 18 \Omega$ ; (b)  $L_0 = 135$  mH,  $C_0 = 25$  mF,  $R_{HF} = 0.35 \Omega$ ,  $R_{LF} = 9 \Omega$ ,  $R_d = 0.6 \Omega$  and  $C_d = 98$  mF.

We have also computed the impedance of the CNU and proposed equivalent circuit models that accurately predict the CNU performance across a wide frequency spectrum. Our simulation results compare well with existing measured Nyquist and CV plots.

### Appendix . Simulation methodology

This appendix describes the three key components in our simulation: scaling, Coulomb interaction and boundary conditions, and particle dynamics.

#### A.1. Scaling

We approximate the 3D CNT ‘forest’ by a 2D equivalent. This dimensional transformation preserves the volume density (using the concept of super-particle), ionic momentum and acceleration, ensemble average drift velocity, ionic collision period, and capacitor current density. Once this set of conditions is imposed, we can then obtain  $R_{sim} = R_{exp}$ ,  $C_{sim} = C_{exp}/k_0$ , and  $L_{sim} = L_{exp}/k_0$ , where  $k_0$  is the scaling

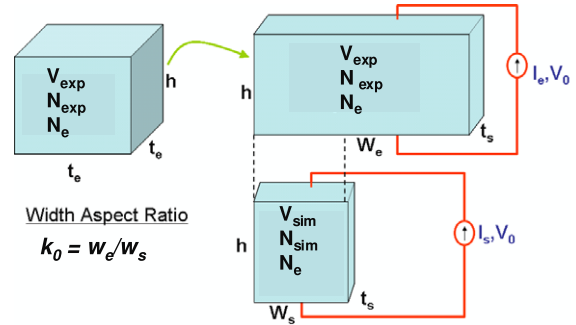


**Figure A.1.** Schematic of the geometrical transformation of the actual electrolyte cell to an effective 2D cell, which is then scaled to an equivalent 2D simulation unit cell with scaling factor  $k_0$ .  $t_s$  is the average electrolyte ion separation and represents the simulation cell thickness. The 3D cell width,  $w_e$ , is determined from  $w_e t_s = t_e^2$ . The electrolyte ion volume density in the actual cell,  $N_e = 6 \text{ mol l}^{-1}$ , is preserved during this transformation.  $N_{exp}$  and  $N_{sim}$  are the numbers of ions in the actual and simulated cell volumes, respectively. The simulation cell dimensions are  $w_s = 1.5 \mu\text{m}$  and  $h = 3 \mu\text{m}$ .

**Table A.1.** Scaling relationships between the actual and simulation cells.  $k_0$  is the scaling factor defined in figure A.1.

Experiment	Simulation
$\tau$	$\tau$
$N_e$	$N_e$
$V_{drift}$	$V_{drift}$
$F_{tot}$	$F_{tot}k_0$
$q$	$qk_0$
$m$	$mk_0$
$R$	$R$
$L$	$L/k_0$
$C$	$C/k_0$
$f$	$fk_0$

factor defined in figure A.1 and  $R_{sim}$ ,  $R_{exp}$ ,  $C_{sim}$ ,  $C_{exp}$ ,  $L_{sim}$ , and  $L_{exp}$  are the measured and simulated CNU resistances, capacitances, and inductances, respectively. The transformation of the 3D UC cell to a 2D unit cell is shown in figure A.1. From the scaling relations given above, the frequency scales as  $f_{sim} = k_0 f_{exp}$ . Table A.1 summarizes the scaling relations for all the parameters used in our simulations.

During the simulation, we also need to preserve the experimental electrolyte volume density,  $N_e$ . To do so, we calculate the experimental electrolyte ‘one-ion volume’ and scale it linearly to the simulated volume, which is assumed to be ‘one-ion’ thick. The simulation cell thickness  $t_s$  shown in figure A.1 is calculated by linearly scaling the electrolyte volume density to a single ion. If  $N_{exp}$  and  $N_{sim}$  are the numbers of ions in the experimental and simulated cell volumes  $V_{exp}$  and  $V_{sim}$ , respectively, we then have  $N_e = N_{exp}/V_{exp} = N_{sim}/V_{sim}$ , ensuring that  $N_e$  is preserved throughout. From the definition of  $k_0$ , we obtain  $N_{exp} = k_0 N_{sim}$ . To preserve the total ion mass and charge between experiment and simulation, each simulated ion (super-particle) must have mass and charge  $k_0$  times larger than those of the ion in the experimental electrolyte ion. This implies that the number of actual ions (positive or negative) in each super-particle in the simulation cell is  $k_0$ . Thus the

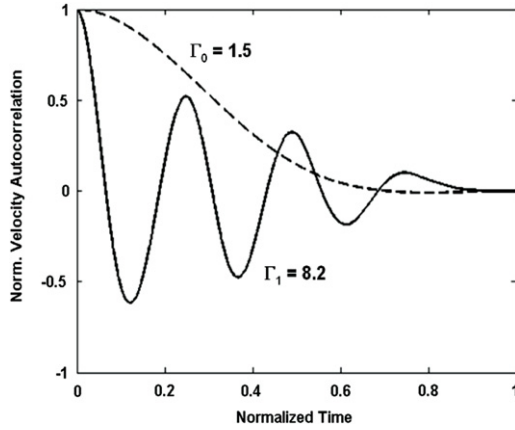


**Figure A.2.** Simulated results for a system of negatively charged ions surrounded by periodic boundary walls. The normalized velocity autocorrelation of the electrons in the system is calculated as a function of time for two different ionic areal densities with ratio  $n_0/n_1 = 10000$ . The time scale is normalized to 0.1 ps for  $\Gamma_1$  and to 10 ps for  $\Gamma_0$  [19].

drift current characteristics in the simulated unit cell are consistent with the experimental electrolyte particle density since the mass to charge ratio of the electrolyte remains constant between experiment and simulation.

### A.2. Coulomb interaction and boundary conditions

We assume a CNT in a unit cell surrounded by rigid walls on the horizontal boundaries and periodic boundary conditions on the vertical cell boundaries, as shown in figure A.1. The rigid wall serves as a reflection plane and energy is conserved during the elastic reflection. The Coulomb interaction must be treated using periodic boundary conditions. The most plausible implementation utilizes the minimum image approximation, derived from the Ewald sum method [19].

To ensure proper accounting for the Coulomb interaction, two tests have been performed. First, the MD algorithm is tested with two different plasma coupling coefficients  $\Gamma = e^2(\pi n)^{1/2}/(4\pi\epsilon k_B T)$ , where  $n$  is the particle areal density,  $k_B T$  is the average kinetic (thermal) energy, and  $\epsilon$  is the dielectric constant. According to [19, 31], the velocity autocorrelation of electrons in a low  $\Gamma$  environment decays exponentially with time but is oscillatory at high  $\Gamma$ . We study the cases  $\Gamma_0 = 1.5$  (low-density) and  $\Gamma_1 = 8.2$  (high-density), as illustrated in figure A.2, and confirm the reported behaviors [19]. We have also confirmed that the electrostatic potential between the capacitor electrodes is independent of path selection. In fact, for two independent paths the electric potential energies is computed to be within 0.24% of each other. Thus the total energy is conserved in our computations [19].

### A.3. Particle dynamics

The unit cell is filled with the electrolyte, KOH, and an ac voltage is applied across the electrodes. The total

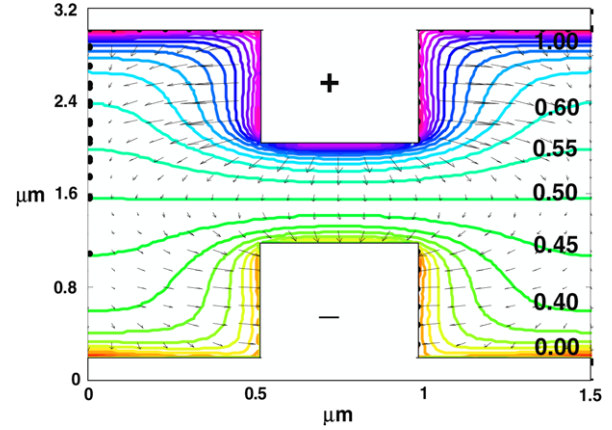


**Figure A.3.** Normalized potential contour plot and electric field lines in the simulated CNU cell for OCV = 0.6 V. The top electrode is positively charged and the bottom electrode is negatively charged.

current density ( $J_{\text{tot}}$ ) is then calculated as the time and ensemble averages of the electrolyte drift current ( $J_{\text{drf tot}}$ ) plus the displacement current between the CNU electrodes ( $J_{\text{dsp.}}$ ), with the total drift component expressed as  $J_{\text{drf tot}} = J_{\text{drf}}(\text{K}^+) - J_{\text{drf}}(\text{OH}^-)$  in  $J_{\text{tot}} = J_{\text{drf tot}} + J_{\text{dsp.}}$ . The field created by the CNT electrodes is determined by separately analyzing the electrodes in a damping MD mode [19]. Therefore, the applied voltage is manifested as electrode charges fixed at designated locations and each charge oscillates as  $q(t) = q_0 \cos(\omega t)$ . Figure A.3 shows the electric field lines and normalized potential contours in the capacitor for an electrode charge distribution at 0.6 V. The CNT and the capacitor horizontal metallic walls are equipotential surfaces.

We employ the concept of a ‘super-particle’, a massive and highly charged ion. Under this assumption, the total force on the massive super-particle is determined by the applied voltage and the total friction in the electrolyte. Starting from the total force on a single ion, we formulate the equations of motion for the super-particle as follows:

$$\vec{F}_i = m_i \vec{A}_i = q_i \vec{E}_i - \frac{m_i \vec{v}_i}{\tau} + \sum_j \frac{e^2}{4\pi\epsilon R_{ij}^3} \vec{R}_{ij} \quad (\text{A.1})$$

$$\sum_i \vec{F}_i = \sum_i m_i \vec{A}_i = \sum_i q_i \vec{E}_i - \sum_i \frac{m_i \vec{v}_i}{\tau} + \sum_{i \neq j} \sum_j \frac{e^2}{4\pi\epsilon R_{ij}^3} \vec{R}_{ij} \quad (\text{A.2})$$

$$\vec{F}_{\text{tot}} = Q \vec{E}_{\text{av}} - \frac{M \vec{v}_{\text{av}}}{\tau}, \quad Q = k_0 q_i, \quad M = k_0 m_i. \quad (\text{A.3})$$

Here  $\tau$  is the collision period in the electrolyte,  $\vec{v}_{\text{av}}$  is the center-of-mass velocity,  $\vec{v}_i$  is the drift velocity,  $m_i$  is the electrolyte ion mass,  $q_i$  is the electrolyte ion charge,  $A_i$  is the electrolyte ion acceleration,  $\vec{E}_i$  is the electric field strength,  $\vec{F}_i$  is the electrolyte ion force,  $Q$  is the center-of-mass charge,  $M$  is the super-particle mass,  $\vec{E}_{\text{av}}$  is the center-of-mass electric field, and  $\vec{R}_{ij}$  is the electrode-to-electrolyte-ion distance. Equation (A.1) describes the general force equation on a single particle. In equations (A.2) and (A.3), the electrolyte

Coulombic force does not influence the center-of-mass motion of the super-particle. The total force on the electrolyte ions given by equation (A.3) consists of contributions only from the electric field and dynamic friction. The last term in equation (A.2) vanishes in the limit of a very large super-particle,  $k_0 \rightarrow \infty$ . From the variables defined above,  $\tau$  and  $k_0$  are the only required inputs to the MD simulation and are obtained from experiment [17].  $\tau$  is extracted from the real part of the impedance  $Z(\omega)$  of an experimental Nyquist plot. The simulation is performed in a time-domain iterative process during which the total force per electrolyte particle is calculated based on the electrode applied voltage acceleration and electrolyte friction deceleration, with the new displacement computed accordingly. Thus the total current in the CNU cell is computed for a given voltage, from which the impedance characteristics are obtained.

## References

- [1] Lee S W, Junhyung Kim J, Shuo Chen S, Hammond P T and Shao-Horn Y 2010 *ACS Nano* **4** 3889
- [2] Miller J R, Outlaw R A and Holloway B C 2010 *Science* **329** 1637
- [3] Peres R N M, Guinea F, Neto C A H, Novoselov K S and Geim A K 2009 *Rev. Mod. Phys.* **81** 109
- [4] Koetz R and Carlen M 2000 *Electrochem. Acta* **45** 2483
- [5] Liu C, Yu Z, Neff D, Zhamu A and Jang B Z 2010 *Nano Lett.* **10** 4863
- [6] Kim J et al 2008 *Nano Lett.* **8** 1813
- [7] Sterk Z, Bugavinovic S, Dekanski A and Rajcic-Vujasinovic M 2010 *Acta Phys. Polon.* **117** 228
- [8] Siddiqui S, Arumugam P U, Chen H, Li J and Meyyappan M 2010 *ACS Nano* **4** 955
- [9] Ngo Q, Cruden B A, Cassell A M, Sims G, Meyyappan M, Li J and Yang C Y 2004 *Nano Lett.* **4** 2403
- [10] Chmiola J, Yushin G, Gogotsi Y, Porter C, Simon P and Taberna P L 2006 *Science* **313** 1760
- [11] Orphanou A, Yamada T and Yang C Y 2011 *Material Research Society Spring Meeting* vol M10.9 (San Francisco, CA, April) p 165
- [12] Chmiola J, Lagreot C, Taberna P-L, Simon P and Gogotsi Y 2010 *Science* **328** 480
- [13] In J H, Kumar S, Yang S H and Barbastathis G 2008 *Appl. Phys. Lett.* **88** 083104
- [14] Chen P C, Shen G, Sukcharoenchoke S and Zhou C W 2009 *Appl. Phys. Lett.* **94** 043113
- [15] Schindall J 2007 *IEEE Spectr.* **44** 42–6
- [16] Zhou R, Meng C, Zhu F, Li Q, Liu C, Fan S and Jiang K 2010 *Nanotechnology* **21** 345701
- [17] Frackowiak E, Metenier K, Bertagna V and Beguin F 2000 *Appl. Phys. Lett.* **77** 2421
- [18] Conway B E and Pell W G 2003 *J. Solid State Electrochem.* **7** 637
- [19] Yamada T and Ferry D K 1993 *Phys. Rev. B* **47** 6416
- [20] Pauling L 1970 *General Chemistry* (San Francisco, CA: Freeman)
- [21] Dresselhaus M S, Dresselhaus G and Avouris Ph (ed) 2001 *Carbon Nanotubes* (Berlin: Springer)
- [22] Sorescu D C, Jordan K D and Avouris P 2001 *J. Phys. Chem.* **105** 11227
- [23] Ricca A and Drocco J A 2002 *Chem. Phys. Lett.* **367** 217
- [24] Bauschlicher C W Jr and Ricca A 2004 *Phys. Rev. B* **70** 115409
- [25] Yamada T 2006 *Appl. Phys. Lett.* **88** 083106
- [26] Frackowiak E and Beguin F 2002 *Carbon* **40** 1775
- [27] Kim C and Yang K S 2003 *Appl. Phys. Lett.* **83** 1216
- [28] Chen J H, Li D Z, Wang D Z, Yang S Z, Wen J G and Ren Z F 2002 *Carbon* **40** 1193
- [29] Pech D, Brunet M, Durou H, Huang P, Mochalin V, Gogotsi Y, Taberna P L and Simon P 2010 *Nature Nanotechnol.* **5** 651
- [30] Lee S W, Yabuuchi N, Gallant B M, Chen S, Kim B S, Hammond P T and Shao-Horn Y 2010 *Nature Nanotechnol.* **5** 531
- [31] Jacoboni C and Reggiani L 1985 *Rev. Mod. Phys.* **55** 645